ISSN 1062-8738, Bulletin of the Russian Academy of Sciences: Physics, 2025, Vol. 89, No. 5, pp. 661–669. © Pleiades Publishing, Ltd., 2025.

Ionospheric Manifestations of a Moderate Geomagnetic Storm on September 12, 2023, Based on Comprehensive Ionospheric Radiosonde Data

F. I. Vybornov[a, d, *], E. Yu. Zykov[b], A. A. Kolchev[b], and I. V. Krasheninnikov[c]

[a] *Radiophysical Research Institute, Nizhny Novgorod State University, Nizhny Novgorod, 603950 Russia*

[b] *Kazan (Volga Region) Federal University, Kazan, 420008 Russia*

[c] *Pushkov Institute of Terrestrial Magnetism, Ionosphere and Radio Wave Propagation, Russian Academy of Sciences, Moscow, 108840 Russia*

[d] *Volga State University of Water Transport, Nizhny Novgorod, 603950 Russia*

**e-mail: vybornov@nirfi.unn.ru*

Received November 26, 2024; revised December 23, 2024; accepted January 31, 2025

Abstract—Results are presented from studies of the ionosphere on September 12, 2023, performed by a system of mid-latitude synchronously operating oblique and vertical sounding ionosonde stations. Strong diffuse reflections from dynamic structures of the auroral ionosphere are detected against the background of regular reflections from the F-layer of the ionosphere during the main phase of the development of a class G1 geomagnetic storm.

Keywords: ionosphere, geomagnetic disturbances, ionosonde, chirp sounding, shortwave radio communication, absorption, scattering of radio waves

DOI: 10.1134/S1062873825710979

INTRODUCTION

The basic tool for diagnosing and monitoring the state of the ionized part of the Earth's atmosphere is vertical incidence sounding (VIS) of the ionosphere. The result is the recording of a VIS ionogram—the frequency dependence of the group delay of the probing signal on the frequency. A substantially less applicable technique is oblique radiosonding (OIS), due to the greater complexity of generating and interpreting the radiophysical response in the form of OIS ionograms. The conditions of reflection for probing radio waves from ionospheric irregularities in the vertical and oblique radio sounding of the ionosphere differ considerably, which in the case of their joint application can provide expanded experimental data on the evolution of such large-scale dynamic structures as traveling ionospheric disturbances (TID) [1] and specific auroral inhomogeneities of the high-latitude ionosphere. The auroral part of the high-latitude ionosphere is characterized by large-scale dynamic irregularities: the polar oval, the main ionospheric trough (MIT), and the auroral D- and E-layers, which can shift to the mid-latitude region and manifest in ionospheric radiosonde data during ionospheric disturbances caused by magnetic storms.

Ionospheric manifestations of geomagnetic disturbances strongly affect the propagation of short radio waves through the ionospheric plasma. This results in increased absorption, smaller ranges of frequencies of transmission up to complete blocking (blackouts), scattering on inhomogeneities of electron density (turbulence) in the region of the polar oval, the emergence of anomalous modes, and deviation of the directions of signal arrival from the arc of a great circle between the transmitter and receiver [2–7]. The strong effect of geomagnetic disturbances have on the efficiency of radio engineering systems has been noted (see, e.g., [8–10]) when the negative phase of a magnetic storm and strong absorption generated by charged particles in the E and D layers of the ionosphere cover large regions where shortwave radio communication and over-the-horizon radar paths can pass. To varying degrees, these effects of ionospheric disturbances have also been observed in data from complex measurements made on September 12, 2023, under conditions of a moderate geomagnetic storm.

Results on the effect of a weak ionospheric storm on the transauroral radio path of the Norilsk–Irkutsk meridional orientation were presented in [11], using data from vertical and oblique radio sounding of the ionosphere. The aim of this work was to develop complex registration capabilities of the oblique and vertical radio sounding of the ionosphere in the problem of diagnosing dynamic large-scale inhomogeneities of

Table 1. Coordinates of LFM stations

No.	LFM Stations	Coordinates
1	Vasilsursk (T)	56.1° N; 46.0° E
2	Kazan (R, T)	55.8° N; 49.1° E
3	Nizhny Novgorod (R)	56.3° N; 44.0° E
4	Troitsk (R)	55.5° N; 37.3° E

Table 2. Parameters of probing paths

No.	Path	Length, km	Azimuth, deg
1	Vasilsursk–Kazan	193	100.7
2	Vasilsursk–Nizhny Novgorod	130	279.7
3	Vasilsursk–Troitsk	555	266.2
4	Kazan–Nizhny Novgorod	323	282.7
5	Kazan–Troitsk	743	272.3

ionospheric plasma through the localization of measuring instruments in the latitudinal direction; to describe the experiment and the heliogeophysical conditions; and to present and discuss our results.

DESCRIPTION OF THE EXPERIMENT AND HELIOGEOPHYSICAL CONDITIONS OF OBSERVATIONS

The experiment was performed using the facilities of Nizhny Novgorod State University's Lobachevsky Radiophysical Research Institute in Kazan (Volga Region) and Institute of Terrestrial Magnetism, Ionosphere and Radio Wave Propagation, Russian Academy of Sciences (IZMIRAN, Troitsk, Moscow). The geometry of the ionospheric diagnostic network paths using linear frequency modulated (LFM) signals and our description of the technology and equipment basically repeats those given in [9]. LFM OIS stations in Vasilsursk transmitted, those in Troitsk and Nizhny Novgorod received, and those in Kazan transmitted and received. Vertical sounding ionosondes were also operating in Vasilsursk (CADI; in 6-min operating mode) and in Troitsk (Parus-A, in the standard 15-min mode). A diagram of the relative positions of the ionosondes is presented in Fig. 1a.

The coordinates of the LFM sounding stations are given in Table 1. Symbols R and/or T indicate settings for receiving and/or transmitting, respectively. Table 2 presents geometric data in the OIS ionosphere configuration, i.e., the lengths of the radio sounding paths and azimuths from the point of transmission to the reception point.

The LFM stations in Vasilsursk, Kazan, and Nizhny Novgorod were of the same type (SITCOM LLT, Yoshkar-Ola) with a maximum radiated power of 100 W. Different antennas were used. In Vasilsursk, the Delta antenna was oriented to the north; in Kazan, the Naklonny Luch antenna was oriented to the west. A vertical Delta antenna was used in Nizhny Novgorod, and a vertical dipole (without azimuth directionality) was used in Troitsk.

On September 12, 2023, LFM stations began transmitting at 15:00 Moscow time (MT). Transmissions from Kazan were made on even minutes, and those from Vasilsursk were made on odd minutes. On September 13, LFM stations transmitted from 17:30 MT in 3-min cycles (but not at the zero minute). The Kazan and Vasilsursk LFM stations switched on in the first and second minutes, respectively, and the cycle was repeated. The speed of operating frequency tuning was 110 kHz/s in the range of 4 to 12 MHz, allowing OIS ionograms in to be recorded in a minute regime. The stations in Nizhny Novgorod and Troitsk received LFM radiation every minute, while those in Kazan and Vasilsursk received it in the intervals of cycles where the stations did not transmit.

Figure 1b shows the geophysical situation on September 12 and 13, 2023, according to data from [12, 13]. A moderate magnetic storm began on September 12, 2023, with an increase in the magnetic index D_{st} at 00:00 UT. The initial phase lasted until 12:00 UT on 12.09.2023, when there was a sharp drop in index D_{st} The main phase of the storm then began and continued until 23:00 UT, where a value of –85 nT was reached. This was followed by the start of the recovery phase.

Geomagnetic disturbance index Kp at the start of the day on September 12, 2023, was at a level of 0–1. It began to grow after 9:00 UT and reached a level of 5+ from 12:00 UT to 18:00 UT. The Kp index then began to fall [12, 13]. The most sensitive ground-based indicator of the intensity of magnetic disturbances was auroral index *AE*, which showed strong variations on September 12. From 11:00 UT to 13:00 UT, the *AE* values rose to 800–1000 nT. Starting at 16:00 UT, they rose to 1900 nT in less than an hour and then began to fall gradually [12].

(a)

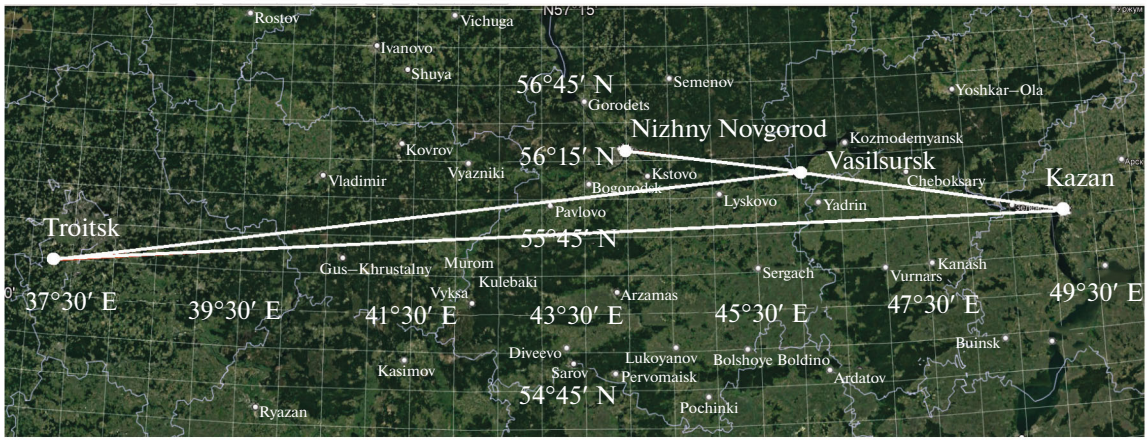

(b)

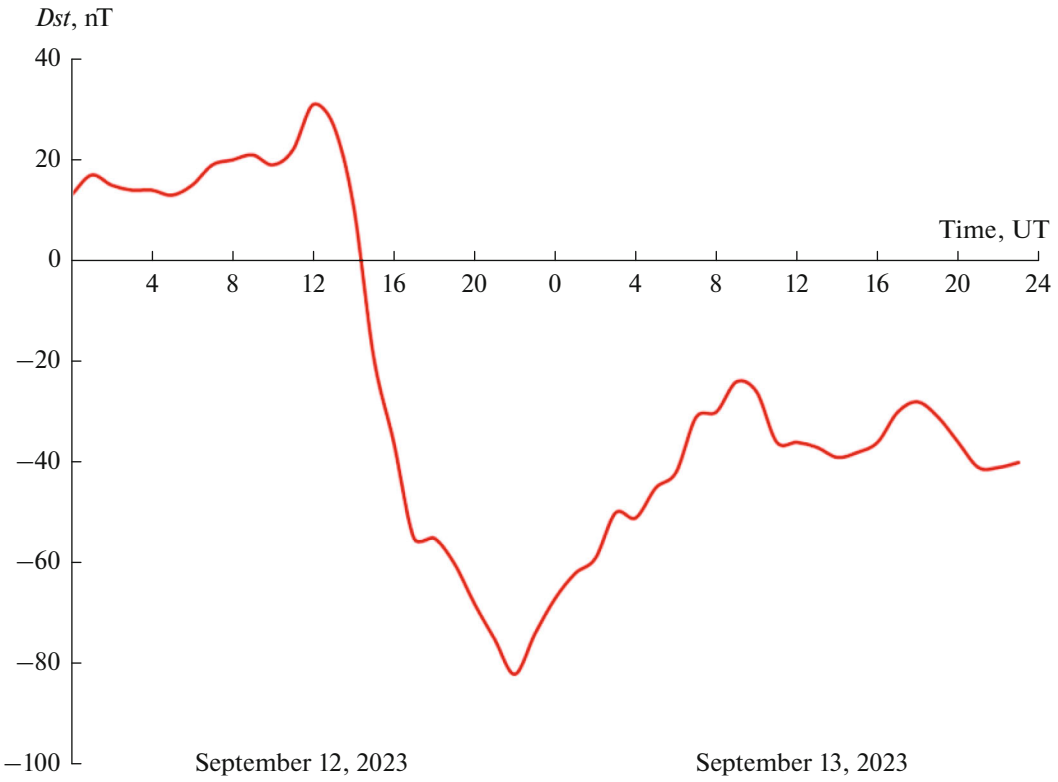

Fig. 1. (a) Scheme of the mutual arrangement of the ionosondes. (b) Magnetic index *Dst* of September 12–13, 2023.

Unfortunately, we were unable to to perform a behavioral analysis of the B_z components of the interplanetary magnetic field (data from the ACE satellite were outside the range of registration). The geomagnetic storm was accompanied by optical phenomena. Aurora borealis with a pronounced green component were recorded in Nizhny Novgorod oblast (including at the NIRFI-Vasilsursk test site) on the night of September 12–13, 2023.

Solar flare activity was generally low for September 10–12. Only type C flares were observed on September 10, the largest being the C8.3 flare from active region AR3423 at 01:41 UT. Weak coronal mass ejections (CMEs) were recorded during the day. Solar

activity rose to moderate levels on September 11, due to three M-type flares. The M1.3 flare in AR3429 at 01:08 UT produced a CME east of the Sun (as viewed from Earth) that had no effect on the ionosphere. The most likely cause of the geomagnetic storm that began on September 12 was apparently a coronal mass ejection at 22:35 UT on September 11, accompanied by the speed of high-speed solar wind streams (CP HSS, Coronal Hole High Speed Streams) rising from 340 to 450 km/s.

Outbreak activity was moderate on September 12, 2023. Three M-type flares and 11 C-type flares occurred during the day. Three coronal mass ejections were observed by the LASCO C2 coronagraphs on board the SOHO spacecraft. At least two of them (at 19:12 UT and 21:12 UT) were apparently on the far side of the Sun, so they had no effect on the Earth.

OBSERVATION RESULTS

LFM OIS stations began work at 16:00 MT, according to the agreed program. DFCs in the F-layer of the ionosphere were reliably recorded on all sounding paths until 19:00, which is typical of an undisturbed ionosphere (see Figs. 2a, 2b, 3a, and 3d).

Reception of LFM Transmitter Signals from Vasilsursk (Figs. 2a–2e)

Additional tracks on the OS ionograms were recorded on the Vasilsursk–Nizhny Novgorod path (see Figs. 2a and 2b). Weak scattered reflections with 6–8 ms periods of delay appeared at 18:55 MT, when the maximum usable frequency (MUF) of the 1F ionosphere (determined everywhere from the ordinary component) was 7.5 MHz and traces of the 2F–4F modes were recorded well. Diffuse reflection in the 7–9 MHz range of frequencies was recorded in the form of a double cloud with delays of 6–6.5 and 7–7.5 ms.

At 18:59 MT, the delays fell to 5–6 and 6.2–8 ms with a 6.8–11 MHz range of frequencies. The areas of scattering began to contrast strongly. The region of scattering was adjacent to track 2F on the high-frequency side. MUF 1F of the ionosphere did not change.

At 19:01 MT, the delays fell to 5–7.5 ms with a 7.5–11 MHz range of frequencies. The region of scattering became uniform with contours similar to those of track 1F. At 19:05 MT, the delays fell to 4–6.5 ms with a 6–12 MHz range of frequencies. MUF 1F rose to 7.8 MHz. At 19:07 MT, the delays fell to 3.5–6.5 ms. The formation of a second scattering track with a delay of 4 ms and a lower frequency of 8 MHz began. MUF 1F rose to 8 MHz. Delays fell to 3–5 ms starting at 19:09 MT. The intensity (contrast on DFC) of the scattered signal grew until 19:17 MT, with MUF 1F remaining close to 8 MHz. The intensity of the scattered signal fell until 19:29 MT, with MUF 1F dropping to 7.8 MHz.

The behavior of the DFC ionosphere on the Vasilsursk–Kazan path (see Figs. 2c and 2d) was generally reminiscent of the dynamics of the DFC behavior on the Vasilsursk–Nizhny Novgorod path. The emergence of a scattered area was noted from 18:59 MT in the range of 7.5–10 MHz with delays of 5–7.5 ms and MUF track 1F at 8.2 MHz. The shape of a diffuse trace characteristic of an oblique reflection from a highly inhomogeneous region (with signs of upper rays) was much more pronounced. By 19:29 MT, MUF 1F had falklen to 8 MHz, and the contrast of the region of scattering was becoming weak.

An additional flat diffuse layer with delays of 4–5 ms and a 4 to 9 MHz range of frequencies appeared above the main region of scattering on the DFC (OIS ionogram) starting at 19:07 MT. It rose weakly up to frequencies of 6 MHz by 19:29 MT. A similar weak layer with similar parameters existed on the DFC path Vasilsursk–Nizhny Novgorod. Note that the delays of this track were 1–1.5 ms longer than those of the main region of scattering. An additional weak diffuse track was recorded with the same periods of delay but in the 9–11.5 MHz range of frequencies starting at 19:21 MT.

The behavior of the DFC ionosphere on the Vasilsursk–Troitsk path (see Figs. 2d and 2e) had a number of interesting features. Higher MUF values than on other paths (rising from 8.5 MHz at 18:55 to 9.3 MHz at 19:11 MT with a subsequent drop to 8.5 MHz at 19:29 MT). A region of scattering with delays greater than 7 ms appeared at 18:59 MT in the 9.5–10.5 MHz range of frequencies (the entire DFC was limited to 10 MHz). A diffuse layer characteristic of oblique reflection formed at 19:05 MT with a 4.5–6.5 ms range of delays in the 7–11 MHz range of frequencies. The region of scattering was divided in two at 19:09 MT. The upper part had delays of 4.8–7.5 ms in the 7–9 MHz range of frequencies, while the lower one had delays of 4–5 ms in the 7–11 MHz range of frequencies. The maximum range of frequencies the lower region of scattering was recorded at 19:11 MT: 8–12 MHz.

The areas of scattering started to contrast less and were faintly visible on the DFC. The upper region of scattering had 5–6.5 ms intervals of delay and a 5–8 MHz range of frequencies. The values for the lower region were 4–5 ms and 8.5–11 MHz, respectively.

Receiving Signals from the LFM Transmitter in Kazan (Figs. 3a–3e)

It should be noted that intense signals of regular reflections (1F–4F) were received on the Kazan–Nizhny Novgorod (Figs. 3a–3c) and Kazan–Troitsk (Figs. 3g–3e) paths. However, the scattered signals were received more weakly than when the LFM signals transmitter in the village of Vasilsursk was operating, due to the features of the directional pattern of the transmitting antenna.

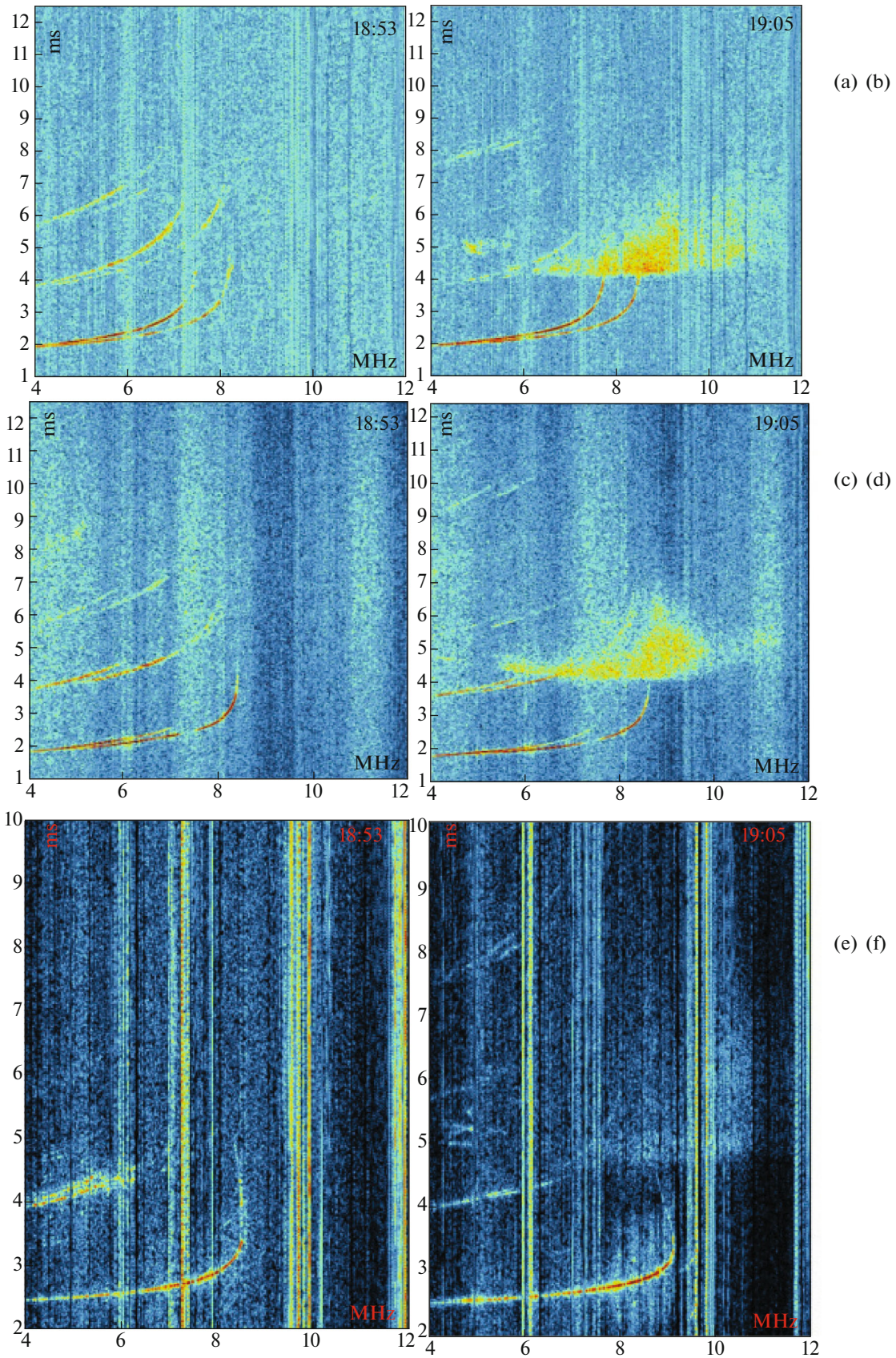

Fig. 2. DFC ionosphere on paths Vasilsursk–Kazan (a, b); Vasilsursk–Nizhny Novgorod (c, d); Vasilsursk–Troitsk (d, e) on September 12, 2023, at 18:53 and 19:05, MT.

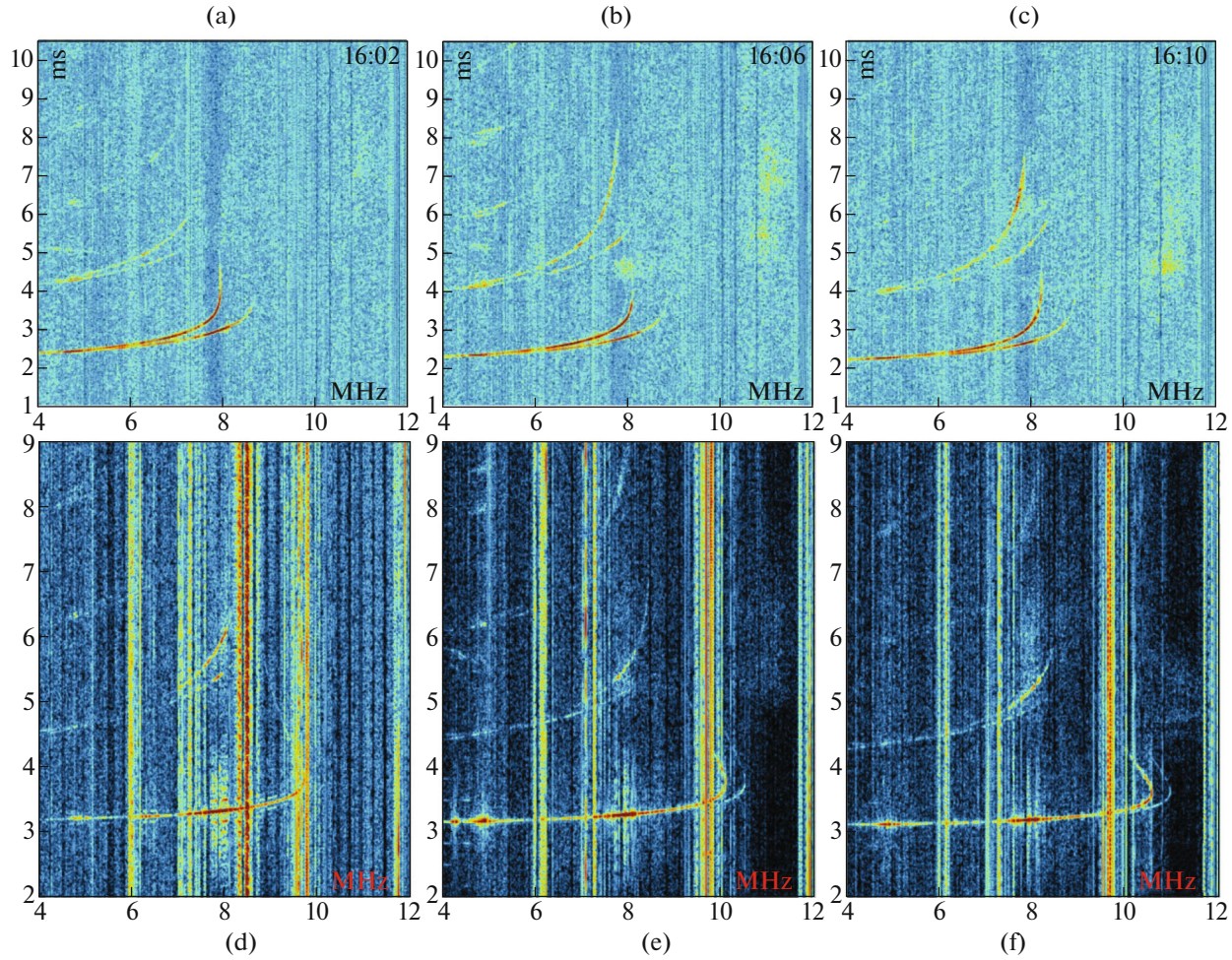

Fig. 3. DFC ionosphere on paths Kazan–Nizhny Novgorod (a–c); Kazan–Troitsk (g–e) September 12, 2023, at 16:02, 16:06, and 16:10 UT.

Two diffuse areas with frequencies of 7–9 and 10.5–11.5 MHz and delays of 4–5 and 4.5–6.5 ms appeared on the Kazan–Nizhny Novgorod radio path at 19:04 MT. At this time, the MOF was around 8 MHz. It rose to 8.1 MHz at 19:14 MT, and fell to 7.5 MHz by 19:24 MT. At 19:24 MT, two regions of scatterings were observed weakly at frequencies of 7.5–8 and 10.5–11.5 MHz with delays of 3.5–5 and 4.5–5.5 ms. No scattering was recorded after 19:30 MT.

The MOF was 9.7 MHz on the Kazan–Troitsk path in the 19:02 MT session. It rose to 10.3 MHz at 19:14 MT and fell to 10.0 MHz at 19:24 MT. A region of scattering appeared at 19:06 MT at frequencies of 10.5–11.5 MHz with delays of 5–7 ms. At 19:08 MT, it acquired a diffuse inclined form of regular reflection with a low frequency of 8 and a high frequency of 12 MHz. The range of delays was 4.5–6 ms. At 19:14 MT, a second region of scattering formed at frequencies of 7–9 MHz with delays of 5.5–6 ms. By 19:24 MT, the region of scattering registered weakly at frequencies of 10.5–11.5 MHz with delays of 4.5–5.5 ms. It was not observed at subsequent DFCs.

LFM sounding of the ionosphere along the same paths during the control evening time of 17:30 to 20:00 MT on September 13, 2023, did not reveal any region of scatterings on the DFC.

Vertical Sounding of the Ionosphere (Figs. 4a–4e)

At ionosonde CADI (Vasilsursk, Nizhny Novgorod oblast), a region of scattering arose at 19:36 MT (16:36 UT) against a background of regular reflections with a 7.8 MHz critical frequency of the ionospheric F-layer. The region of scattering was observed in the 3.5–6.5 MHz range of frequencies at effective altitudes of 400–750 km. The parameters of the region of scattering changed (2.2–4.4 MHz, 420–700 km) as the critical frequency fell to 5 MHz at 20:00 MT.

At ionosonde Parus-A (IZMIRAN), the critical frequency of the F-band ionosphere was 8.3 MHz at

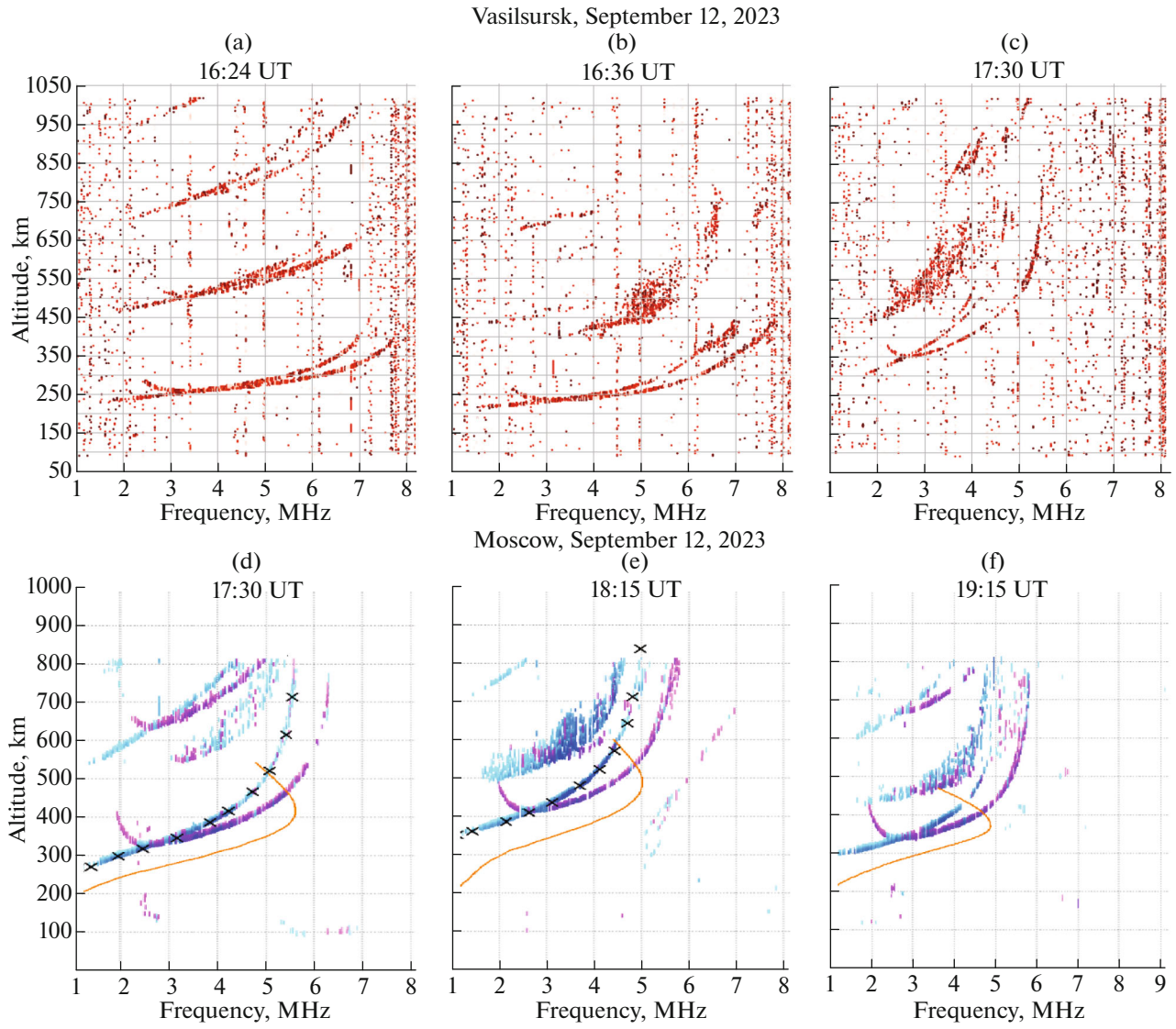

Fig. 4. Ionograms of the vertical sounding of the ionosphere, obtained on September 12, 2023, on the CADI ionosonde in Vasilsursk at 16:24, 16:36, and 17:30 UT (a–c); and at the IZMIRAN station at 17:30, 18:15, and 19:15 UT (g–e).

18:15 MT. There were no signs of disturbances on the ionogram. Diffuseness of 1–2 points of the first and second reflections was observed on the ionogram at 18:30 MT, and was repeated periodically on subsequent ionograms. The critical frequency of the F-layer was 7 MHz at 21:00 MT.

RESULTS AND DISCUSSION

It is known [14, 15] that the effects of geomagnetic activity appear first at high latitudes as a result of magnetospheric–ionospheric interaction under conditions of increased solar wind and precipitation of charged particles. In the auroral ionosphere, three large-scale structures can be identified that manifest in radiosonde data via refractive reflection (geometrical optics): the MIT polar wall, polarization jets (SAID, Sub-Auroral Ion Drifts), and the auroral E-layer. At 17:30, 18:15, and 19:15 UT on September 12, 2023, the polar oval and the MIT polar wall were at the latitude of St. Petersburg with some dynamics to the south (calculations were made as in [16]). (VIS ionograms are presented in Fig. 4.) This made the distance from the IZMIRAN ionosonde ~500 km (5° along the meridian). However, if we estimate the distance from the ionosonde of some large-scale structure of the auroral ionosphere that produces an additional diffuse trace between 1F2 and 2F2 on the VIS ionogram (Fig. 4e), it would be only ~250–300 km at a frequency of 3 MHz, if we allow for measurements of the effective altitude. This is clearly insufficient to explain such a reflection by the MIT polar wall. The auroral E-layer of the ionosphere (formed by the ionization of particles at altitudes of 100–150 km) also cannot be

considered a source of high-intensity reflection, due to the smoothness of its decline in the meridional direction. In that mechanism, there would be virtually no frequency dependence in the trace it forms, and this clearly does not fit with the nature of the experimental recording. Based on general estimates, the most likely source of the formation of the additional trace on these ionograms from VIS stations IZMIRAN and Vasilsursk was therefore a polarization jet [17–19] and accompanying processes in the form of SAR (Stable Auroral Red) arcs [20]—areas with elevated plasma temperatures localized south of the MIT polar wall. This assumption is supported by the strong similarity between the forms of the trace at the IZMIRAN and Vasilsursk stations, which are separated by ~550 km in longitude (Table 2). It is also worth noting the unusual nature of the trace: it lay within the range of frequencies of the base trace formed on the equatorial (background) part of the MIT. This feature of the trace is consistent (at least qualitatively) with a relatively weak drop in electron density in a polarization jet and SAR arcs, and their relatively small cross-sectional size (~100 km). Ionization in the region of the MIT polar wall is normally much stronger than in its equatorial part, so the quasi-critical frequencies are higher when reflected from it.

The delay of additional reflection signals is much longer in the results from oblique radio sounding in the longitudinal direction: on average, it is ~2 ms (600 km) (at the level of the trace of the second multiple reflection from the regular F-layer). It should also be noted that there is a very large excess in the maximum observed frequency, MLF. On average, it is ~2 MHz, which is consistent with the nature of the reflection from the MIT polar wall but contradicts the VIS results (Fig. 4). This is especially evident on the longer Vasilsursk–Troitsk and Kazan–Troitsk radio paths (Figs. 2 and 3), in the form of a low intensity trace. The sliding reflection mechanism for the latitudinal direction of the OS radio paths with large meridional gradients of electron density contributes to earlier registration of additional modes than in VIS. The dynamic mode of auroral origin is therefore clearly visible for the OIS data (16:05 UT, Fig. 2e), while there are no additional traces at all in the VIS data of the IZMIRAN station. We may therefore assume that the two means of ionospheric radio sounding recorded reflections from different large-scale structures of the auroral ionosphere: a polarization jet (VIS) and the MIT polar wall (OIS).

In addition to geometrical optical reflections, ionospheric abnormalities of different scales that are generated in turbulent dynamic regions of the auroral ionosphere can scatter radio signals and produce the aspect (resonance) mechanism of their formation, resulting in the diffuse nature of non-standard traces on ionograms.

CONCLUSIONS

Results from experimental studies of the mid-latitude and subauroral ionosphere using oblique LFM and vertical pulse sounding with a set of radiophysical diagnostic tools localized in the latitudinal direction have been presented for the first time. It was shown that during the main phase of a magnetic storm on September 12, 2023, intense additional signals were observed by a network of synchronously operating LFM stations. These signals were presumably formed by complex mechanisms of reflection from large-scale abnormalities in the auroral ionosphere: a polarization jet and the polar wall of the main ionospheric trough.

ACKNOWLEDGMENTS

The authors thank Senior Researcher M.G. Deminova (Institute of Terrestrial Magnetism, Ionosphere and Radio Wave Propagation, Russian Academy of Sciences) for discussing our results, and Senior Researcher O.A. Sheiner (Lobachevsky Radiophysical Research Institute) for his assistance in analyzing our heliophysical data. We are also grateful to Junior Research Fellow A.V. Pershina (Lobachevsky Radiophysical Research Institute) and Senior Researchers A.M. Padokhina and V.N. Shubina (Institute of Terrestrial Magnetism, Ionosphere and Radio Wave Propagation, Russian Academy of Sciences) for their assistance in this work.

FUNDING

This work was supported by ongoing institutional funding. No additional grants to carry out or direct this particular research were obtained.

CONFLICT OF INTEREST

The authors of this work declare that they have no conflicts of interest.

REFERENCES

1. Krasheninnikov, I.V. and Lyannoi, B.E., *Geomagn. Aeron.*, 1991, vol. 31, no. 3, p. 427.
2. Wagner, L.S., Goldstein, J.A., Rupar, M.A., and Kennedy, E.J., *Radio Sci.*, 1995, vol. 30, no. 3, p. 659.
3. Angling, M.J., Cannon, P.S., Davies, N.C., et al., *Radio Sci.*, 1998, vol. 33, no. 1, p. 97.
4. Milan, S.E., Lester, M., Jones, T.B., and Warrington, E.M., *J. Atmos. Sol.-Terr. Phys.*, 1988, vol. 60, p. 617.
5. Uryadov, V.P., Ponyatov, A.A., Kurkin, V.I., et al., *Radiophys. Quantum Electron.*, 2004, vol. 47, no. 12, p. 933.
6. Vybornov, F.I. Kolchev, A.A., et al., *Adv. Space Res.*, 2018, vol. 61, no. 7, p. 1837.
7. Uryadov, V.P., Vybornov, F.I., and Pershin, A.V., *Radiophys. Quantum Electron.*, 2019, vol. 62, no. 2, p. 85.

8. Uryadov, V.P., Vybornov, F.I., and Pershin, A.V., *Radiophys. Quantum Electron.*, 2021, vol. 64, no. 2, p. 77.
9. Astafyeva, E., Yasyukevich, Y.V., Maletckii, B., et al., *J. Geophys. Res.: Space Phys.*, 2022, vol. 127, no. 1, p. e2021JA029843.
10. Vybornov, F., Sheiner, O., Kolchev, A., et al., *Atmosphere*, 2022, vol. 13, no. 1, p. 84.
11. Kurkin, V.I., Polekh, N.M., and Zolotukhina, N.A., *Geomagn. Aeron.*, 2022, vol. 62, nos. 1–2, p. 104.
12. https://wdc.kugi.kyoto-u.ac.jp.
13. http://www.swpc.noaa.gov.
14. Nishida, A., *Geomagnetic Diagnosis of the Magnetosphere*, Physics in Chemistry and Space, Berlin: Springer, 1978.
15. Uryadov, V.P., Vybornov, F.I., Kolchev, A.A., et al., *Radiophys. Quantum Electron.*, 2017, vol. 60, no. 5, p. 355.
16. Deminov, M.G. and Shubin, V.N., *Geomagn. Aeron.*, 2018, vol. 58, no. 3, p. 348.
17. Stepanov, A.E., Gololobov, A.Yu., Kobyakova, S.E., and Khalipov, V.L., *Radiophys. Quantum Electron.*, 2022, vol. 65, no. 1, p. 9.
18. Stepanov, A.E., Gololobov, A.Yu., Khalipov, V.L., and Golikov, I.A., *Geomagn. Aeron.*, 2021, vol. 61, no. 1, p. 68.
19. Sinevich, A.A., Chernyshov, A.A., Chugunin, D.V., et al., *Geomagn. Aeron.*, 2023, vol. 63, no. 6, p. 747.
20. Rees, M.H. and Roble, R.G., *Rev. Geophys.*, 1975, vol. 13, no. 1, p., 201.